THE JOURNAL OF BIOLOGICAL CHEMISTRY VOL. 291, NO. 52, pp. 26698–26706, December 23, 2016

Substrate Trapping in Crystals of the Thiolase OleA Identifies Three Channels That Enable Long Chain Olefin Biosynthesis*

Received for publication, September 27, 2016, and in revised form, October 31, 2016 Published, JBC Papers in Press, November 4, 2016, DOI 10.1074/jbc.M116.760892

Brandon R. Goblirsch, Matthew R. Jensen, Fatuma A. Mohamed, Lawrence P. Wackett, and Carrie M. Wilmot[1]

From the Department of Biochemistry, Molecular Biology, and Biophysics and Biotechnology Institute, University of Minnesota, St. Paul, Minnesota 55108

Edited by Norma Allewell

Phylogenetically diverse microbes that produce long chain, olefinic hydrocarbons have received much attention as possible sources of renewable energy biocatalysts. One enzyme that is critical for this process is OleA, a thiolase superfamily enzyme that condenses two fatty acyl-CoA substrates to produce a β-ketoacid product and initiates the biosynthesis of long chain olefins in bacteria. Thiolases typically utilize a ping-pong mechanism centered on an active site cysteine residue. Reaction with the first substrate produces a covalent cysteine-thioester tethered acyl group that is transferred to the second substrate through formation of a carbon-carbon bond. Although the basics of thiolase chemistry are precedented, the mechanism by which OleA accommodates two substrates with extended carbon chains and a coenzyme moiety—unusual for a thiolase—are unknown. Gaining insights into this process could enable manipulation of the system for large scale olefin production with hydrocarbon chains lengths equivalent to those of fossil fuels. In this study, mutagenesis of the active site cysteine in *Xanthomonas campestris* OleA (Cys^{143}) enabled trapping of two catalytically relevant species in crystals. In the resulting structures, long chain alkyl groups (C_{12} and C_{14}) and phosphopantetheinate define three substrate channels in a T-shaped configuration, explaining how OleA coordinates its two substrates and product. The C143A OleA co-crystal structure possesses a single bound acyl-CoA representing the Michaelis complex with the first substrate, whereas the C143S co-crystal structure contains both acyl-CoA and fatty acid, defining how a second substrate binds to the acyl-enzyme intermediate. An active site glutamate ($Glu\beta^{117}$) is positioned to deprotonate bound acyl-CoA and initiate carbon-carbon bond formation.

A diminishing, finite fossil fuel supply has prompted the search for alternative energy platforms and new precursor sources for synthesis of complex, high value commodity chemicals. Production of renewable, energy-rich hydrocarbons and their derivatives is at the epicenter of this effort. Cultivating specialized microbes that produce hydrocarbons represents one attractive option (1). Recently, bacteria across multiple phyla have been shown to be capable of generating long chain, olefinic hydrocarbons ranging in size from C_{23} to C_{33} (2). A total of four olefin (*ole*) biosynthesis genes *oleABCD* are clustered within the bacteria capable of this specialized biosynthesis. Bioinformatic analysis has identified *oleB*, *oleC*, and *oleD* genes as members of the α/β-hydrolase, AMP-dependent ligase, and short chain dehydrogenase superfamilies, respectively (3). The *oleA* gene is a member of the condensing or thiolase enzyme superfamily (4, 5).

In vitro studies have demonstrated that OleA, OleD, and OleC enzymes are sufficient for long chain olefin production from acyl-CoA substrate (6). The OleA enzyme initiates biosynthesis by producing a long chain β-ketoacid product that is further processed by OleD to generate a β-hydroxyacid product, with OleC subsequently producing the end point olefin. The exact role of the *oleB* gene product is currently unknown. The OleA, OleD, and OleC enzymes have been individually characterized (6–8). Solution studies on *Xanthomonas campestris* OleA revealed the enzyme efficiently catalyzes so called "head-to-head" condensation between the thioester groups of two long chain fatty acids (C_8-C_{16}) charged in the form of acyl-CoA (6). The mechanism of carbon-carbon bond formation proceeds in a non-decarboxylative fashion between the α-carbon of one substrate to the acyl-carbon of the second (6). The overall reaction generates two free CoA molecules and a single β-ketoacid product that becomes the substrate of OleD (7).

Thiolase superfamily enzymes begin turnover by acylation of an active site cysteine (9). A second substrate then binds, and condensation can proceed. The crystal structure of OleA from *X. campestris* has been determined and consists of the typical homodimeric thiolase protein fold (10). Because OleA catalyzes the condensation of two large substrates with long hydrophobic alkyl moieties, each OleA monomer was predicted to contain three extended substrate channels centered on the active site cysteine (Cys^{143} in *X. campestris* OleA). The pantetheinate channel, common to all thiolases, would coordinate the phosphopantetheine moiety of each successive acyl-CoA substrate. The two alkyl channels each bind a single alkyl moiety: one associated with the acylated active site cysteine and the other with the second acyl-CoA substrate. In other well studied and

* This work was supported by National Institutes of Health Chemistry Biology Interface Training Grant GM-008700 (to M. R. J.), the Department of Energy (Advanced Research Projects Agency - Energy) under Award DE-AR0000007 (to L. P. W.), a University of Minnesota Biotechnology Institute grant (to C. M. W. and L. P. W.), and University of Minnesota Doctoral Dissertation Fellowship (to B. R. G.). The authors declare that they have no conflicts of interest with the contents of this article. The content is solely the responsibility of the authors and does not necessarily represent the official views of the National Institutes of Health.

The atomic coordinates and structure factors (codes 4KTI, 4KTM, 4KU2, 4KU3, and 4KU5) have been deposited in the Protein Data Bank (http://wwpdb.org/).

[1] To whom correspondence should be addressed. Tel.: 612-624-2406; Fax: 612-625-5780; E-mail: wilmo004@umn.edu.

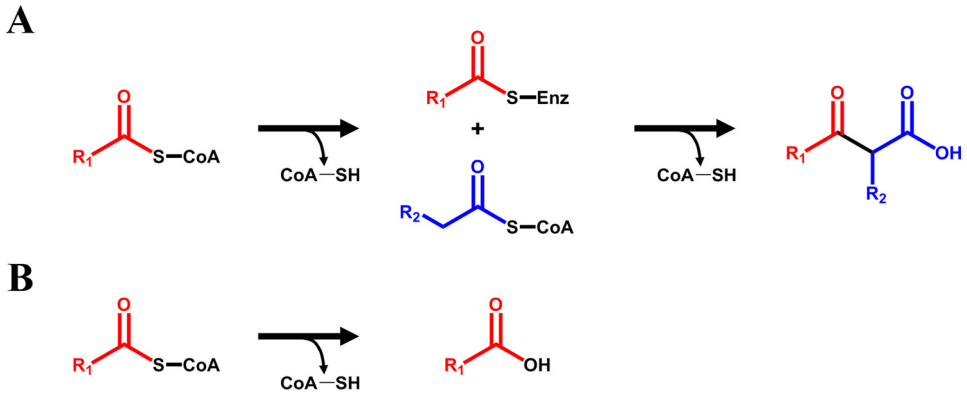

FIGURE 1. **OleA-catalyzed reactions with acyl-CoA substrates.** *A*, condensation of acyl-CoA substrates to produce β-ketoacid product. *B*, direct hydrolysis of acyl-CoA substrate.

structurally characterized thiolase superfamily enzymes, such as β-ketoacyl-acyl carrier protein synthases (11–13), polyketide synthases (14), and HMG-CoA synthase (15) at least one of the substrates is small, and so two alkyl channels are not necessary. Of the currently characterized thiolase superfamily enzymes, only OleA and some of the pyrone and pseudopyrone ketosynthases, such as the recently identified *Pseudomonas* sp. GM30 pseudopyronine synthase, are likely to require three distinct substrate channels (16, 17). The previously described crystal structure of OleA in complex with the covalent inhibitor, cerulenin, which has a C_8 hydrocarbon tail, has suggested the position of one of the two alkyl channels (10).

In this study, we have determined the crystal structures of the catalytically impaired C143A and C143S OleA co-crystallized with acyl-CoA substrate. These structures define substrate binding and validate our previously postulated three channel configuration (10). The position of amino acids in the active site relative to substrate coordination suggests a revised mechanism that includes a glutamate donated by the other monomer (Gluβ^{117} in *X. campestris* OleA): a novel feature of OleA.

Results

Expression and Purification of WT, C143A, and C143S OleA Enzymes—Heterologously expressed C143A and C143S OleA were purified in yields similar to the WT enzyme (6). On average, 1 g of wet cell pellet yielded 750 μg of OleA enzyme. Purity of the sample was confirmed by SDS-PAGE. Electrospray ionization-MS was performed after each purification to ensure the expected mutation had been introduced. The WT, C143A, and C143S OleA had experimental molecular masses of 38,661.8, 38,630.0, and 38,645.8 Da, corresponding well to the predicted masses of 38,661.2, 38,629.2, and 38,645.2 Da, respectively.

Activity of C143A and C143S OleA toward Myristoyl-CoA Substrate—A colorimetric assay using 5,5′-dithio-*bis*-(2-nitrobenzoic acid) (DTNB)[2] was adapted to measure OleA turnover (6, 18, 19). The assay measures production of free CoA, which can be produced either by proper condensation or futile hydrolysis of the thioester bond of acyl-CoA substrates (Fig. 1). *X. campestris* OleA has been previously shown to prefer C_{16} and C_{14} acyl-CoA substrates (6). The C_{14} acyl-CoA substrate, myristoyl-CoA, was selected for DTNB assays to compare WT and mutant OleA turnover. Table 1 summarizes the myristoyl-CoA consumption by WT and OleA enzyme variants. WT OleA enzyme displays robust turnover. Conversely, C143A and C143S OleA display measurable CoA release only after incubation for 24 h.

TABLE 1
Wild type and mutant OleA consumption of myristoyl-CoA
The values shown are the averages in triplicate with standard deviations.

Enzyme	Enzyme concentration	Rxn time	CoA product[a]	Percent yield[b]
	μM	*h*	μM	%
WT	0.5	0.25	33 ± 0.5	100
C143A	0.5	0.25	<0.1	<0.1
C143A	0.5	24	0.8 ± 0.4	2.5
C143A	0.5	48	5 ± 0.3	15
C143S	0.5	0.25	0.1 ± 0.07	0.3
C143S	0.5	24	0.4 ± 0.3	1.3
C143S	0.5	48	4 ± 0.08	13

[a] Free coenzyme A was detected as described under "Experimental Procedures."
[b] The starting substrate was 32 μM. 32 μM product is 100% turnover.

Overall Structures of OleA Cys^{143} Variants—The structures of unbound C143A and C143S OleA were determined to 1.85 and 2.36 Å resolution, respectively (Table 2). The gross structure of the homodimer of each variant is nearly superimposable with the WT enzyme structure. The calculated root mean square deviation (rmsd) for all backbone atoms between OleA WT and each variant structure are 0.14 (C143A) and 0.19 Å (C143S).

Past attempts at generating WT OleA co-crystal structures with non-covalent ligands (CoA; myristic acid) or trapping *in crystallo* catalytic intermediates from myristoyl-CoA turnover were unsuccessful, yielding only unbound enzyme. Crystal soaking experiments were also unsuccessful, presumably because of the large ligand and substrate sizes. The minimal activity of C143A and C143S OleA variants with myristoyl-CoA (Table 1) suggested that co-crystallizations were feasible. Co-crystallization of C143A OleA with myristoyl-CoA and C143S OleA with lauroyl-CoA or myristoyl-CoA generated crystals of a new, bi-pyramidal morphology. Although multiple acyl-CoA lengths were tried in co-crystallization experiments (C_8-C_{16}), only lauroyl-CoA (C_{12} acyl-CoA) and myristoyl-CoA (C_{14} acyl-CoA) produced co-crystals. Furthermore, C143A OleA did not co-crystallize with lauryl-CoA. The structures of C143A OleA-

[2] The abbreviations used are: DTNB, 5,5′-dithio-*bis*-(2-nitrobenzoic acid); rmsd, root mean square deviation; Fab, fatty acid biosynthesis; ACP, acyl carrier protein; APS, Advanced Photon Source.

TABLE 2

C143A and C143S data collection statistics

The data in parentheses are for the highest resolution shell.

	C143A OleA	C143S OleA	C143A OleA-myristoyl-CoA co-crystal	C143S OleA-myristoyl-CoA co-crystal	C143A OleA-lauroyl-CoA co-crystal
Data collection					
Wavelength (Å)	1.03	1.54	1.03	1.03	1.03
Space group	$P2_12_12_1$	$P2_12_12_1$	$P2_12_12_1$	$P2_12_12_1$	$P2_12_12_1$
Unit cell (Å)	84.2 × 85.5 × 103.7	81.9 × 85.5 × 102.0	81.7 × 85.7 × 101.7	81.4 × 85.9 × 101.7	81.4 × 85.5 × 101.6
Resolution (Å)	50.0–1.85 (1.88–1.85)	50.0–2.36 (2.40–2.36)	50.0–1.98 (2.01–1.98)	50.0–1.97 (2.00–1.97)	50.0–2.17 (2.21–2.17)
Measured reflections	463702	211791	415958	390033	263108
Unique reflections	61827	30076	50726	51928	38581
Completeness (%)	98.3 (97.2)	99.7 (96.6)	100 (100)	100 (100)	100 (100)
R_{merge} (%)[a]	7.3 (44.4)	6.3 (33.6)	5.5 (41.7)	7.7 (52.2)	10.9 (57.5)
I/σ_I	23.6 (6.5)	20.5 (3.1)	29.7 (4.7)	23.9 (4.3)	18.2 (3.5)
Multiplicity	7.5 (7.6)	7.0 (5.8)	8.2 (8.2)	7.5 (7.5)	6.8 (6.8)
Wilson B factor (Å^2)	23.0	29.4	28.1	27.2	29.7
Source	APS sector 23	In house	APS sector 23	APS sector 23	APS sector 23
Refinement					
Resolution (Å)	44.0–1.84 (1.87–1.84)	32.8–2.36 (2.44–2.36)	31.6–1.98 (2.01–1.97)	44.0–1.94 (1.98–1.94)	44.0–2.17 (2.22–2.17)
R_{work}[b]	0.153	0.166	0.157	0.154	0.159
R_{free}[c]	0.200	0.218	0.199	0.196	0.203
Ramachandran statistics (%)[b]					
Favored	97.17	97.11	97.54	97.80	97.67
Outliers	0	0	0	0	0
rmsd					
Bond lengths (Å)	0.015	0.003	0.030	0.007	0.009
Bond angles (°)	1.546	0.777	1.694	1.089	1.372
Average B-factor (Å^2)	22.9	37.8	36.0	33.3	34.0
Ligand B-factor (Å^2)[d]			55.8	39.8/40.0	50.1/42.8
Clashscore[e]	4.23	3.17	4.01	4.59	4.26
Protein Data Bank ID	4KTI	4KTM	4KU2	4KU3	4KU5

[a] $R_{merge} = \Sigma_i|I_{hkl,i}| - \{I_{hkl}\}/\Sigma_{hkl}\Sigma_i I_{hkl,i}$, where I is the observed intensity, and $\{I_{hkl}\}$ is the average intensity of multiple measurements.
[b] $R_{work} = \Sigma||F_o| - |F_c||/\Sigma|F_o|$, where $|F_o|$ is the observed structure factor amplitude, and $|F_c|$ is the calculated structure factor amplitude.
[c] R_{free} is the R factor based on 5% of the data excluded from refinement.
[d] Myristoyl-CoA/lauroyl-CoA and myristic acid/lauric acid average ligand B-factor data are separated by a virgule, respectively.
[e] Based on values obtained from MolProbity (31).

TABLE 3

Overview of bound channels of reported structures and rmsd from WT OleA

The root mean square deviation values were calculated over all backbone atoms between structures by SUPER in PyMOL.

Crystal	PDB ID	Channel ligands	Channels bound	rmsd from WT OleA
				Å
C143A	4KTI	None	None	0.14
C143S	4KTM	None	None	0.19
C143A Myristoyl-CoA	4KU2	Myristoyl-CoA	Alkyl channel A, pantetheinate channel	0.32
C143S Myristoyl-CoA	4KU3	Myristoyl-CoA, myristic acid	Alkyl channel A and B, pantetheinate channel	0.38
C143S Lauroyl-CoA	4KU5	Lauroyl-CoA, lauric acid	Alkyl channel A and B, pantetheinate channel	0.32

myristoyl-CoA, C143S OleA-myristoyl-CoA, and C143S OleA-lauroyl-CoA were determined to 1.98, 1.97, and 2.17 Å, respectively (Table 2). Overall, the structure of the homodimer of each co-crystal structure is very similar to WT OleA, with the rmsd of all backbone atoms ≤ 0.38 Å (Table 3).

Our previous studies on OleA led to the proposal that three extended substrate binding channels would be required per monomer to complete OleA turnover: one channel dedicated to coordinating the CoA head group and phosphopantetheine arm (pantetheinate channel) and two channels to coordinate the hydrophobic alkyl chains of the acyl-CoA substrates (alkyl channels A and B) (10). The electron density of the C143A OleA myristoyl-CoA structure demonstrated binding of a single myristoyl-CoA molecule (occupancy = 100%) in which the CoA and its phosphopantetheine arm bound as expected, and the C_{14} alkyl chain lay between a β-sheet and two helices to give an L-shaped binding mode (Fig. 2*A*). This channel is undescribed in the thiolase superfamily, but its existence was previously suggested by the structure of WT OleA in complex with the covalent inhibitor, cerulenin, which has a C_8 alkyl tail, and the position of a xenon atom from a xenon-derivative crystal structure of OleA (10). We have termed this channel alkyl channel A. In the C143S OleA-myristoyl-CoA structure, we observed a noncovalently bound myristic acid (occupancy = 100%) within alkyl channel A, whereas a substrate myristoyl-CoA (occupancy = 88%) was positioned within the pantetheinate channel, but with its alkyl chain bound within a channel whose entrance from the active site is directly opposite that of alkyl channel A (Fig. 2*B*). We term this alkyl channel B. This channel is in the same position as that defined by crystal structures of fatty acid biosynthesis (Fab) β-ketoacyl-acyl carrier protein synthase enzymes; the complex of C112A FabH with lauroyl-CoA (equivalent to C143A *X. campestris* OleA), FabH bound to decane-1-thiol, and FabB bound to cerulenin (11, 20, 21). Note that in the FabB-cerulenin complex, the C_8 alkyl tail of cerulenin binds in alkyl channel B, whereas in OleA, despite alkyl channel B being present, cerulenin occupies alkyl channel A (10, 21). The electron density of C143S OleA-lauroyl-CoA reveals binding of lauric acid (occupancy = 99%) and lauryl-CoA (occupancy = 84%) in positions equivalent to those observed in the C143S OleA-myristoyl-CoA crystal structure (Fig. 2*C*). Overlays between all three co-crystal structures revealed that binding of the CoA portion of all the acyl-CoAs is essentially identical (Fig. 3*A*). Furthermore, the binding of alkyl groups within

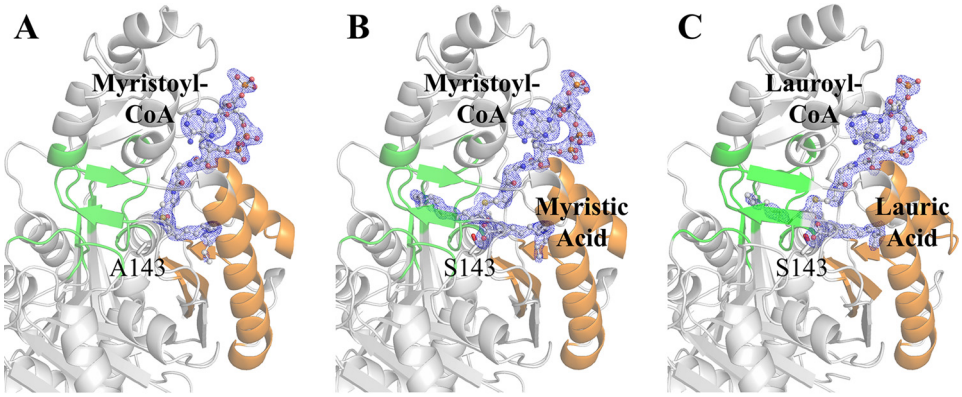

FIGURE 2. **Substrate binding channels in OleA C143 mutants.** *A*, C143A OleA bound with myristoyl-CoA (ball and stick). *B*, C143S OleA bound with myristic acid and myristoyl-CoA. *C*, C143S OleA bound with lauric acid and lauroyl-CoA. The single monomer of OleA is shown in *gray cartoon* with alkyl channels A (*orange cartoon*) and B (*green cartoon*) color-coded for clarity. The mutated residue is shown as a stick model (*gray carbon*). Bound substrates are represented as ball and stick models with *blue mesh* illustrating the simulated annealing ligand omit $F_o - F_c$ electron density maps contoured at 2.5 σ.

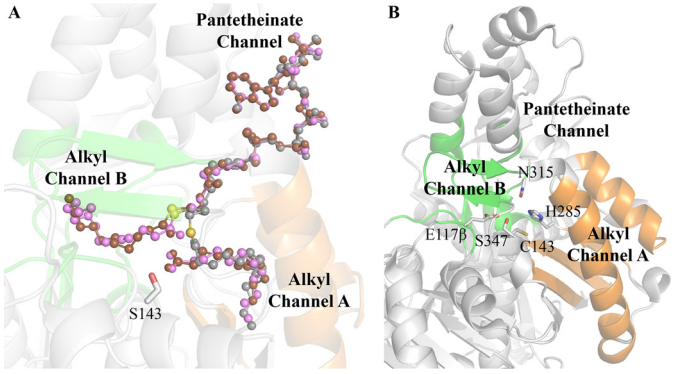

FIGURE 3. *A*, overlay of C143A and C143S co-crystal structures. Bound ligands (ball and stick) are color-coded by structure: C143A-myristoyl-CoA (*gray*), C143S-myristoyl-CoA (*magenta*), and C143S-lauroyl-CoA (*brown*). Sulfur atoms are colored *yellow* for orientation. *B*, OleA WT monomer highlighting the three-channel nexus at the active site. Active site residues are shown as sticks (*gray carbon*). Alkyl channels A and B colored as in Fig. 2.

alkyl channels A and B also occupy comparable positions (Fig. 3*A*). Thus, we can clearly define three extended channels in OleA that together form a T-shaped, three-channel nexus (Fig. 3*B* and Table 3).

The origin of the free fatty acid observed in the C143S OleA complex structures is unclear but likely comes from hydrolysis of a species bound in alkyl channel A. One possibility is hydrolysis of a covalent acyl intermediate generated by ester bond formation between acyl-CoA and deprotonated Ser^{143}. An ester-containing covalent acyl intermediate has previously been observed in an equivalent Cys to Ser variant of the thiolase *Escherichia coli* β-ketoacyl-ACP synthase I (22). Such covalent acyl intermediates have enhanced stability (ester *versus* thioester) and are often observable. However, in the case of C143S OleA, efforts to observe such a species by electrospray ionization-MS or through co-crystallization have failed. The second possibility is hydrolysis of acyl-CoA substrate non-covalently bound in the active site. Regardless of the species hydrolyzed, the end result is a fatty acid tightly bound in alkyl channel A that does not dissociate before a second acyl-CoA binds.

Of note is that only one monomer active site of the OleA dimer in the crystallographic asymmetric unit contains bound fatty acid and/or acyl-CoA in all three OleA variant co-crystal structures, with the other monomer active site showing no evidence of significant binding. Because these are co-crystal structures, this means that dimers in which only one monomer has bound to substrate were selected out by the crystallization process. In contrast, the previously reported WT OleA-cerulenin co-crystals crystallized in a different space group with only a monomer in the asymmetric unit, and thus inhibitor was equally present in both monomers of the dimer generated by crystallographic symmetry (10).

Interactions of Acyl-CoA within the OleA Pantetheinate Channel—The position of the CoA moiety in all acyl-CoA co-crystal structures is conserved (Figs. 2 and 3*A*). Ionic and polar interactions occurring between myristoyl-CoA and C143A OleA are shown as representative of all three structures (Fig. 4*A*). The amine group of the myristoyl-CoA adenine ring forms hydrogen bonds with the hydroxyl group of Thr^{250} and the main chain carbonyl oxygen of Arg^{195}, whereas the 3′ phosphate group forms a hydrogen bond with the hydroxyl group of Thr^{60}. The guanidinium group of Arg^{195} also forms a cation-π stacking interaction with the adenine ring of the acyl-CoA. In OleA, the phosphopantethine group of the acyl-CoA forms no discernable hydrogen bond or ionic contacts with the remainder of the pantetheinate channel leading to the active site.

Active Site Perturbations Induced by Acyl-CoA and Fatty Acid Binding—The active site of OleA features a catalytic cysteine residue (Cys^{143}) lying at the terminus of the pantetheinate channel (Fig. 3*B*). Residues are positioned immediately above Cys^{143} to help stabilize tetrahedral, oxyanionic intermediates formed during OleA turnover. Pockets formed by the side chains of His^{285} and Asn^{315} and the main chain amides of Cys^{143} and Ser^{347} stabilize these intermediates. A glutamic acid ($Glu\beta^{117}$) is also positioned in the active site but unusually originates from the neighboring monomer.

Mutation of the active site Cys^{143} of OleA causes no perturbation of active site residues in the C143A and C143S OleA variant structures. When myristoyl-CoA is bound to C143A OleA, minimal perturbation is observed (Fig. 4*B*). $Glu\beta^{117}$ is positioned in the active site, and hydrogen bonds with the hydroxyl of Ser^{347} and an active site water molecule. Interestingly, the thioester moiety of myristoyl-CoA forms no hydrogen bonds with OleA active site residues and is positioned 5.5 Å away from the Cβ of Ala^{143}. In the C143S-myristoyl-CoA crys-

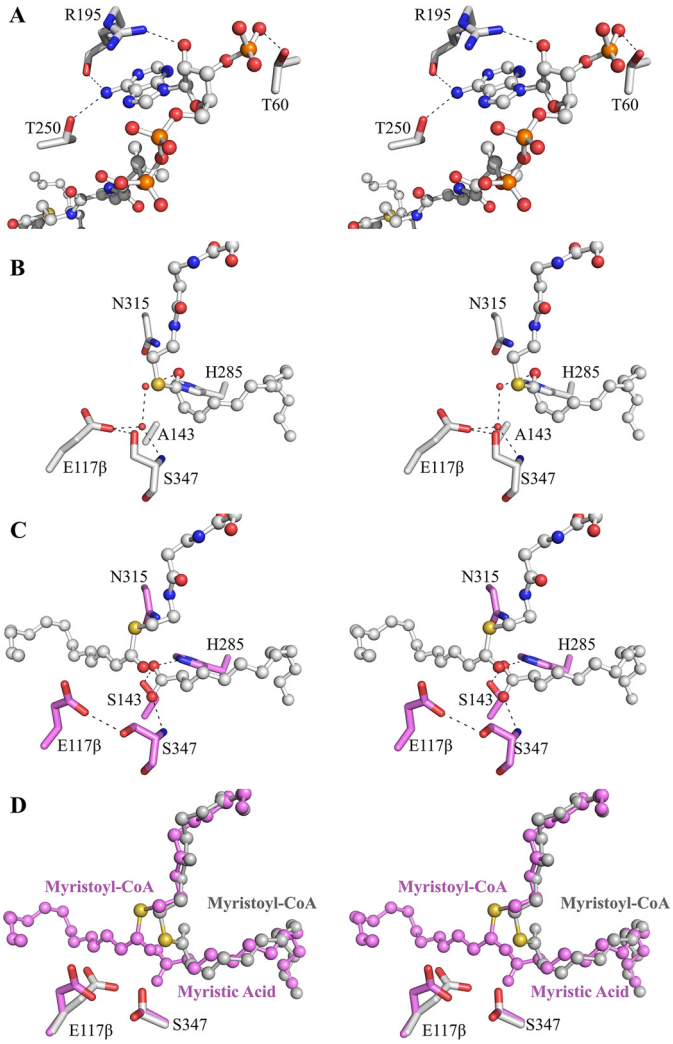

FIGURE 4. **Stereoviews (cross-eyed) of the C143A and C143S myristoyl-CoA co-crystal active sites.** *A*, acyl-CoA bound in the OleA pantetheinate channel. Pantetheinate channel residues forming hydrogen bonds with the CoA moiety are shown as sticks (*gray carbon*). The guanidium group of residue Arg[195] additionally pi-stacks with the adenine ring of coenzyme A. *B*, C143A bound with myristoyl-CoA (ball and stick). Active site residues are shown as sticks (*gray carbon*). *C*, C143S bound with myristic acid and myristoyl-CoA (ball and stick) occupying alkyl channels A and B, respectively. Active site residues are shown as sticks (*pink carbon*). *D*, overlay of C143A and C143S co-crystal structures. Color coding for active site residues are conserved as in *B* and *C*. Bound myristoyl-CoA (*gray*, C143A co-crystal; *pink*, C143S co-crystal) and myristic acid (*pink*, C143S co-crystal) are explicitly labeled. Note significant movement of the side chains of Gluβ^{117} and Ser^{347} occurs to accommodate the alkyl chain in channel B. In all panels, hydrogen bond contacts are represented by *dashed lines*, and the ordered waters are shown as *red spheres*.

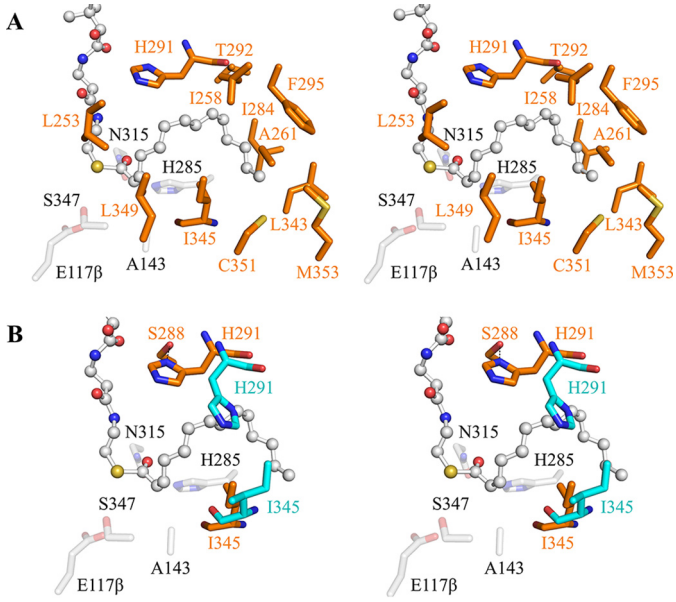

FIGURE 5. **Stereoviews (cross-eyed) of OleA alkyl channel A.** *A*, C143A bound with myristoyl-CoA (ball and stick). Residue side chains forming the channel are indicated by sticks (*orange carbon* and *label*). *B*, overlay of unbound C143A OleA (*blue carbon*) with C143A co-crystallized with myristoyl-CoA (*orange carbon*). Residues His[291] and Ile[345] undergo significant conformational changes to bind myristoyl-CoA. Active site residues are shown as faded sticks (*gray carbon*). Hydrogen bond contacts are represented by *dashed lines*.

tal structure, alkyl channel A is occupied by myristic acid, and a myristoyl-CoA molecule is stacked above with its alkyl chain lying in alkyl channel B (Figs. 2*B* and 4*C*). In this structure, active site waters are completely displaced. The myristic acid carboxylate forms an extensive hydrogen bonding network with the side chains of Ser[143] and His[285] and the main chain amide of Ser[347]. Gluβ^{117} remains hydrogen bonded to Ser[347], but the presence of the alkyl chain from myristoyl-CoA forces an outward rotation of the carboxylate (Fig. 4*D*).

Alkyl Chain Binding Environments in Channels A and B—Alkyl channel A is formed by a pair of α-helices composed of residues 252–272 and 289–301 flanked by a region of β-sheet consisting of residues 280–284, 339–346, and 349–355. The C143A-myristoyl-CoA and C143S-myristoyl-CoA structures have long chain alkyl groups (C_{14}) bound in alkyl channel A. These are highly kinked with their terminal carbon positioned near Cys[351], Met[353], and Phe[295] (Fig. 5*A*). Binding of the hydrocarbon chain in alkyl channel A results in little perturbation with the exception of two amino acid residues. His[291], positioned at the ceiling of the channel, flips out of the pocket and forms a hydrogen bond interaction with Ser[288] (Fig. 5*B*). At the base of the channel, the Ile[345] residue also adopts an alternative rotamer, and the peptide backbone moves deeper into the base of the channel (Fig. 5*B*). The path of the alkyl chain is being driven by the side chain positions of Ile[258], Ile[284], Val[287], and Phe[295], which curls the alkyl moiety around the Ile[345] side chain.

Residues originating from multiple structural elements form alkyl channel B. Two α-helix termini formed by residues 170–177 and 201–207 and three loops consisting of residues 110–114, 239–249, and 315–318 compose the majority of the channel (Fig. 3*B*). A loop from the other monomer of the dimer containing Gluβ^{117} (residues 116–118) completes alkyl channel B. To fit within the channel, the C_7-C_{14} carbons of the myristoyl-CoA alkyl group curve back toward the OleA active site with the final alkyl carbon positioned near Met[246] and Gluβ^{117} (Fig. 6). The base and rear of alkyl channel B also possesses residues with charged/polar side chains that may also encourage the curving of the alkyl chain back upon itself.

Discussion

Intermediate binding steps observed during OleA turnover have previously proved elusive. Whereas the general mechanistic outlines of carbon-carbon bond formation had been estab-

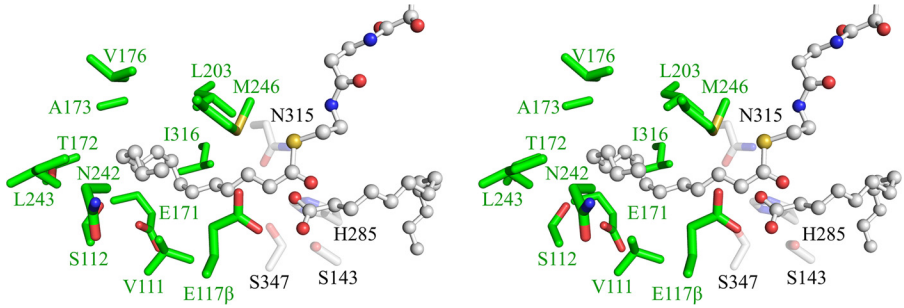

FIGURE 6. **Stereoview (cross-eyed) of OleA alkyl channel B.** C143S OleA bound with myristoyl-CoA (ball and stick) within alkyl channel B. Residue side chains forming the channel are indicated by sticks (*green carbon*). Active site residues are shown as faded sticks (*gray carbon*).

lished, the events surrounding the condensation step were not well understood (4, 6). The non-decarboxylative Claisen mechanism of condensation catalyzed by OleA requires two thioester-acyl groups to be coordinated within the active site simultaneously prior to condensation. A three-channel nexus at the active site was proposed to enable the condensation chemistry to commence (10). The structures presented here validate this model, and allow for the proposal of events before and after condensation. The C143A and C143S OleA variants provided the opportunity to trap acyl-CoA substrate within OleA and provide insight into the workings of these essential channels (Fig. 3 and Table 3).

As in all thiolases, a single pantetheinate channel leads to the active site of OleA. Although the CoA head group makes multiple ionic and hydrogen bond interactions at the surface of OleA, the phosphopantetheine arm of the CoA makes no charged/polar interactions through the remainder of the channel leading to the OleA active site (Fig. 4*A*). This is consistent with the need for uncharged CoASH to have a high dissociation constant enabling efficient release and allowing entry of the second acyl-CoA substrate. Analogously, FabH makes few contacts with the CoA moiety of bound lauroyl-CoA, where release of CoASH is required for the binding of the second substrate, malonyl-ACP (20, 23).

Alkyl channels A and B are perpendicular to the pantetheinate channel and lead away from the active site to create a T-shaped configuration of channels (Fig. 3). OleA represents the first description of alkyl channel A, and its presence in other thiolases with two bulky substrates is likely. In particular, some of the ketosynthases involved in bacterial pyrone biosynthesis create an α-pyrone ring with large orthogonal substituents, including the antibiotics myxopyronin, corallopyronin, and pseudopyronin (17, 24, 25). The orthogonal nature of the substituents matches well with the orthogonal alkyl channels observed in OleA, as was noted in the recent crystal structure of *Myxococcus fulvus* Mx f50 MxnB, the stand-alone ketosynthase that completes myxopyronin biosynthesis (26). The alkyl chains in both OleA alkyl channels A and B are not linear but curled, explaining how different lengths of alkyl chain can be accommodated in the active site and why *X. campestris* OleA is promiscuous (3). The residues lining these channels are not conserved in OleAs, as would be expected given the range of substrate specificity across the enzyme family. A final note is that in both the WT OleA-cerulenin (10) and C143A-myristoyl-CoA structures, alkyl channel A is occupied first (Fig. 2*A*), consistent with this binding the first substrate and thus the covalent acyl-enzyme intermediate prior to condensation. Interestingly, Sucipto *et al.* (26) suggested that in MxnB the first substrate would bind in alkyl channel B based on the steric constraints required for α-pyrone ring formation.

The active site of OleA experiences few changes upon acyl-CoA or acyl-CoA and fatty acid binding (Fig. 4). The bound myristoyl-CoA within C143A OleA rests above the active site residues (Fig. 4*B*). Only solvent molecules remain between the thioester group of myristoyl-CoA and Ala^{143}, suggesting that in WT OleA, descent of myristoyl-CoA to Cys^{143} could readily occur to enable transeserification. The presence of Ser^{143} in the C143S OleA introduces an additional hydrogen bond donor into the active site, which participates in hydrogen bonds to the non-physiological myristic acid head group created by off-pathway hydrolysis (Fig. 4*C*). The binding of the second myristoyl-CoA substrate requires occupation of alkyl channel B and positions the second substrate above the carboxylate of myristic acid. Myristoyl-CoA binding also induces movement of residue $Glu\beta^{117}$ and its hydrogen bond partner Ser^{347} (Fig. 4*D*). The observed stacking of myrisotyl-CoA above myristic acid in OleA mimics the complex between the covalent acyl-OleA intermediate and the second acyl-CoA substrate. Like OleA, HMG-CoA synthase also proceeds through a non-decarboxylative mechanism for carbon-carbon bond formation and contains the same spatially conserved residues in the active site (6, 27). In HMG-CoA synthase, the proton abstraction that initiates carbon-carbon bond formation is catalyzed by an active site glutamate, which is 3.0 Å from the C_2 of the acylated Cys but 5.7 Å from the C_3 of the second substrate acetoacetyl-CoA (15). The carboxylate of $Glu\beta^{117}$ in OleA is spatially equivalent to the HMG-CoA glutamate, but because the alkyl chain of the first substrate occupies channel A, the relevant carbon belonging to the acylated Cys^{143} is now more distant (7.1 Å based on the myristic acid position in the C143S OleA variant complex), and the angle between the carboxylate and the hydrogen makes proton abstraction from this group improbable. However, the carboxylate of $Glu\beta^{117}$ is 4.0 Å away from the α-carbon of the acyl group in alkyl channel B, suggesting that OleA abstracts the proton from the second, non-covalently bound substrate. The interaction with Ser^{347} likely plays a role in activating $Glu\beta^{117}$, promoting abstraction of the acidic proton from the second substrate. The created carbanion would then perform a nucleophilic attack on the acyl-enzyme intermediate to generate the carbon-carbon bond (Fig. 4*C*). In corroboration of this

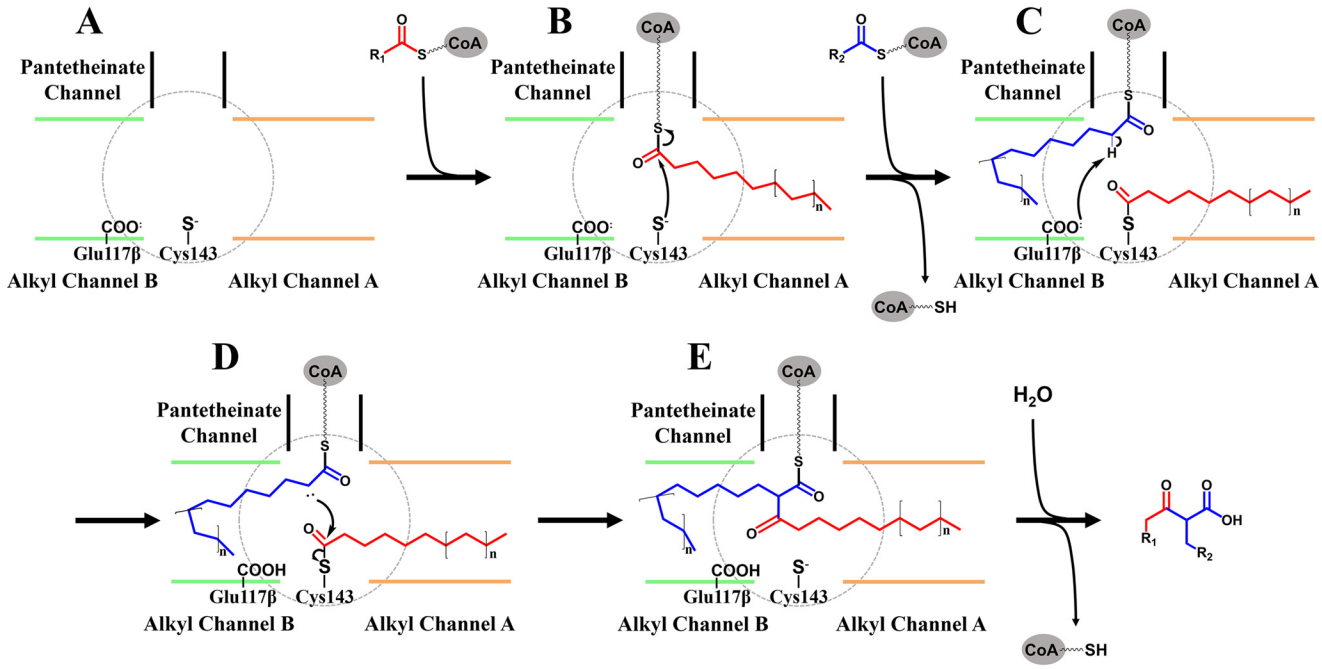

FIGURE 7. **Substrate coordination and proposed reaction scheme of OleA.** The active site of a single monomer is depicted with three substrate channels labeled. Alkyl channel A (*orange*) and alkyl channel B (*green*) are color-coded to be consistent with all previous figures. Coenzyme A is represented by a *gray oval* connected to the phosphopantetheine arm depicted as a *wavy line* terminating in the reactive thiol group. *A*, resting state of OleA. *B*, binding of the first acyl-CoA substrate within alkyl channel A prior to transesterification. The variable length of the alkyl group is signified by *n* repeating units. *C*, binding of the second acyl-CoA substrate within alkyl channel B prior to C–C bond formation. Note a base, putatively assigned as Gluβ^{117}, required to preempt C–C bond formation by proton abstraction. *D*, nucleophilic attack by the α-carbanion of the second acyl-CoA on the thioester of the enzyme-acyl intermediate to form a C–C bond. *E*, bound β-ketoacyl-CoA prior to hydrolysis. The release of free coenzyme A and β-ketoacid product complete OleA turnover back to the resting state.

idea, studies on *Kineococcus radiotolerans* OleA (39% identity with *X. campestris* OleA) have identified a β-ketoacyl-CoA intermediate preceding β-ketoacid formation, which could only occur if the second substrate is activated for nucleophilic attack on the acylated enzyme (7). The combination of the structural data presented here and previous *in vitro* studies leads to the proposal of an updated mechanistic model for OleA turnover (Fig. 7).

Dissociation of the β-ketoacid product is non-trivial because it is so large. It seems likely that the product exits from alkyl channel B, because the β-hairpin (residues 239–249; Fig. 3) that shields the alkyl chain from solvent shows enhanced mobility in the absence of bound ligand (10). The OleA homodimer possesses a pseudo-2-fold axis that places both β-hairpin loops from the monomers in a deep surface groove that contains elements of α-helices in other thiolase superfamily structures (Fig. 8). OleA produces a hydrophobic β-ketoacid product that is labile and unlikely to be released into the cytosol (6). Therefore, the open interface of the OleA homodimer raises the intriguing possibility that the subsequent olefin biosynthesis enzyme, OleD, could directly dock with OleA to facilitate product release and acquire the β-ketoacid.

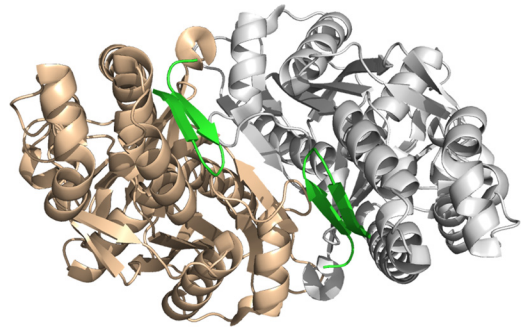

FIGURE 8. **Top-down view of the OleA dimer shown as schematic with each monomer colored coded as *tan* or *gray*.** The loop (residues 238–248) that lies over alkyl channel B is explicitly shown as *green schematic*. The image orientation is ~90° rotation about an axis horizontally in the plane of the paper from the orientation in Fig. 2.

Experimental Procedures

Preparation of OleA Site Mutants C143A and C143S OleA—The cloning of the synthetic *oleA* gene from *X. campestris* spv. campestris str. ATCC 33913 (NP_635607.1) into pET28b+ (Novagen, Madison, WI) was described previously (6). Site specific primers (Integrated DNA Technologies) were designed to mutate the Cys^{143} amino acid in *X. campestris* OleA to a corresponding C143A or C143S. Phusion polymerase (New England Biolabs) was used to generate the mutants via PCR (28). The parental template was removed by digestion with DpnI. Mutagenesis to either C143A or C143S was confirmed by DNA sequencing (ACGT Inc.).

Purification of C143A and C143S OleA—Cultivations of WT OleA and OleA mutants were conducted in 2-liter flasks containing 1 liter of LB medium with 50 μg/ml kanamycin. The BL21 *E. coli* cells (Invitrogen) were induced at an A_{600} of 0.6–0.8 with 0.1 mM isopropyl-β-D-thiolgalactopyranoside. After 4 h, the cells were harvested by centrifugation for 15 min at 4000 × *g*.

The cells were resuspended in 500 mM NaCl, 20 mM sodium phosphate buffer, pH 7.4, with EDTA-free protease inhibitor

tablets (Roche Applied Science). The cells were lysed via a chilled French pressure cell at 20,000 p.s.i. and centrifuged at 27,000 × *g* for 70 min to obtain the soluble fraction. The soluble fraction was then run through a 0.45-μm syringe filter prior to loading onto a ÄKTA FPLC (General Electric) equipped with a 5-ml Ni(II)-loaded His-Trap column equilibrated with 500 mM NaCl, 30 mM imidazole, 20 mM sodium phosphate buffer, pH 7.4. WT OleA and C143A/S point mutants all eluted between 130 and 160 mM imidazole, as monitored by absorbance at 280 nm. Enzyme purity was judged by SDS-PAGE and Simply Blue Safestain (Invitrogen). C143A and C143S OleA variants were further confirmed by mass spectrometry using an Ion-Spray electrospray source coupled to a QSTAR XL (AB Scienx) quadrupole TOF mass spectrometer. All OleA samples were concentrated to between 225 and 300 μM for crystallization trials.

Detection of OleA Turnover of Myristoyl-CoA Substrate—Consumption of myristoyl-CoA (Sigma) substrate during OleA turnover was monitored through quantification of the free thiol group of CoASH product. In the assay, CoASH reacts with DTNB, releasing chromophoric 2-nitro-5-thiobenzoic acid anion, which is measured spectrophotometrically at 412 nm (ϵ_{412} = 13,600 M^{-1} cm^{-1}) (6, 18, 19). OleA enzyme (20 μg) was reacted with 65 μM myristoyl-CoA in 490 μl containing 200 mM sodium chloride, 20 mM Tris HCl, pH 7.4, with 4% (v/v) ethanol, and incubated at room temperature for times ranging from 5 min to 48 h. Each reaction was quenched rapidly by the addition of 4.1 M guanidine HCl at pH 7.4, followed by DTNB addition for 10 min, and then quantification via UV-visible spectrophotometry. Enzyme-dependent consumption of myristoyl-CoA was quantified using the Beer-Lambert Law, controlling individually for background enzyme and substrate (non-enzymatic hydrolysis) contributions to absorbance.

Crystallization of C143A and C143S OleA—Crystallization of WT OleA has been reported previously (10). The C143A and C143S OleA crystals grew from similar conditions. The crystals were grown by hanging drop vapor diffusion at 20 °C. Drops consisted of 1 μl of protein and 1 μl of mother liquor solution (15–20% (w/v) PEG 8000, 70–100 mM potassium phosphate dibasic, and 100 mM sodium citrate, pH 4.2). The crystals were cryoprotected in mother liquor containing 20% PEG 400. Unbound C143A and C143S OleA crystals appeared in 1–3 days and had a rod-like morphology identical to previously characterized WT OleA crystals grown under the same conditions.

C143A and C143S co-crystals were generated by reacting the variant enzyme with 1 mM acyl-CoA substrate (Sigma) for 1 h at 4 °C. Excess acyl-CoA caused phase separation in the crystallization drops, so excess acyl-CoA was removed by a dialysis step prior to setting up the crystallization trays. Co-crystals appeared in 1–4 days with a bi-pyramidal morphology distinct from the unbound OleA crystals.

X-ray Data Collection, Processing, and Refinement—Using 1.03 Å wavelength X-rays, diffraction data sets were collected at National Institute of General Medical Sciences and National Cancer Institute Collaborative Access Team Beamlines 23-ID-D and 23-ID-B of the Advanced Photon Source (APS) (Argonne National Laboratory, Argonne, IL) at 100 K using a MARmosaic 300 CCD. Beam size was adjusted to match the crystal size and orientation and attenuated by 50–150-fold. The data set using X-rays with a wavelength of 1.54 Å was collected on a copper rotating anode X-ray generator (Rigaku) with a Saturn 944+ CCD detector at 100 K at the Kahlert Structural Biology Lab, University of Minnesota. The data collection statistics are listed in Table 2.

All C143A and C143S OleA crystals belonged to space group $P2_12_12_1$ and were isomorphous to the previously reported structure of unbound WT OleA (Protein Data Bank entry 3ROW) (10). The asymmetric unit of the unbound WT OleA consists of a homodimer, and this was used as the initial phasing model in difference Fourier synthesis to solve all mutant structures with PHENIX 1.8.2–1309 (29). The designated R_{free} reflections were carried over from the WT OleA data set. For all structures, cycles of model building with COOT (30) and restrained refinement using PHENIX with TLS were performed until all interpretable regions of the $2F_o - F_c$ and $F_o - F_c$ were explained. All $F > 0\sigma F$ were used in refinement. Refinement statistics were validated using MolProbity (31). All figures illustrating enzyme structures were prepared using PyMOL (32).

Author Contributions—B. R. G. and F. A. M. made the site-directed OleA mutants and purified them. B. R. G. performed all the crystallography. M. R. J. performed the activity assays. B. R. G., C. M. W., and L. P. W. interpreted the data. B. R. G. and C. M. W. drafted the manuscript. C. M. W. and L. P. W. had overall responsibility for the design and coordination of the program. All authors reviewed the results and edited and approved the manuscript.

Acknowledgments—Computer resources were provided by the Basic Sciences Computing Laboratory of the University of Minnesota Supercomputing Institute. X-ray data were collected at the Kahlert Structural Biology Laboratory at the University of Minnesota and National Institute of General Medical Sciences and National Cancer Institute Collaborative Access Team at the APS, Argonne National Laboratory (Argonne, IL). National Institute of General Medical Sciences and National Cancer Institute Collaborative Access Team at the APS has been funded in whole or in part with federal funds from the National Cancer Institute (Grant ACB-12002) and the National Institute of General Medical Sciences (Grant AGM-12006). This research used resources of the Advanced Photon Source, a U.S. Department of Energy Office of Science User Facility operated for the Department of Energy Office of Science by Argonne National Laboratory under Contract DE-AC02-06CH11357. We thank Ed Hoeffner for Kahlert Structural Biology Laboratory support, and the staff at Sector 23, APS for support.

References

1. Wackett, L. P., and Wilmot, C. M. (2015) Hydrocarbon biosynthesis in microorganisms. In *Direct Microbial Conversion of Biomass to Advanced Biofuels* (Himmel, M. E., ed) pp. 442–470, Elsevier, Amsterdam, The Netherlands
2. Sukovich, D. J., Seffernick, J. L., Richman, J. E., Hunt, K. A., Gralnick, J. A., and Wackett, L. P. (2010) Structure, function, and insights into the biosynthesis of a head-to-head hydrocarbon in *Shewanella oneidensis* strain MR-1. *Appl. Environ. Microbiol.* **76,** 3842–3849
3. Sukovich, D. J., Seffernick, J. L., Richman, J. E., Gralnick, J. A., and Wackett, L. P. (2010) Widespread head-to-head hydrocarbon biosynthesis in bacteria and role of OleA. *Appl. Environ. Microbiol.* **76,** 3850–3862

4. Beller, H. R., Goh, E. B., and Keasling, J. D. (2010) Genes involved in long-chain alkene biosynthesis in *Micrococcus luteus*. *Appl. Environ. Microbiol.* **76,** 1212–1223
5. Friedman, L., and Rude, M. (November 13, 2008) U. S. Patent WO 2008/147781 A2
6. Frias, J. A., Richman, J. E., Erickson, J. S., and Wackett, L. P. (2011) Purification and characterization of OleA from *Xanthomonas campestris* and demonstration of a non-decarboxylative Claisen condensation reaction. *J. Biol. Chem.* **286,** 10930–10938
7. Bonnett, S. A., Papireddy, K., Higgins, S., del Cardayre, S., and Reynolds, K. A. (2011) Functional characterization of an NADPH dependent 2-alkyl-3-ketoalkanoic acid reductase involved in olefin biosynthesis in *Stenotrophomonas maltophilia*. *Biochemistry* **50,** 9633–9640
8. Kancharla, P., Bonnett, S. A., and Reynolds, K. A. (2016) *Stenotrophomonas maltophilia* OleC-catalyzed ATP-dependent formation of long-chain Z-olefins from 2-alkyl-3-hydroxyalkanoic acids. *Chembiochem* **17,** 1426–1429
9. Heath, R. J., and Rock, C. O. (2002) The Claisen condensation in biology. *Nat. Prod. Rep.* **19,** 581–596
10. Goblirsch, B. R., Frias, J. A., Wackett, L. P., and Wilmot, C. M. (2012) Crystal structures of *Xanthomonas campestris* OleA reveal features that promote head-to-head condensation of two long-chain fatty acids. *Biochemistry* **51,** 4138–4146
11. Sachdeva, S., Musayev, F. N., Alhamadsheh, M. M., Scarsdale, J. N., Wright, H. T., and Reynolds, K. A. (2008) Separate entrance and exit portals for ligand traffic in *Mycobacterium tuberculosis* FabH. *Chem. Biol.* **15,** 402–412
12. Wang, J., Soisson, S. M., Young, K., Shoop, W., Kodali, S., Galgoci, A., Painter, R., Parthasarathy, G., Tang, Y. S., Cummings, R., Ha, S., Dorso, K., Motyl, M., Jayasuriya, H., Ondeyka, J., *et al.* (2006) Platensimycin is a selective FabF inhibitor with potent antibiotic properties. *Nature* **441,** 358–361
13. Sridharan, S., Wang, L., Brown, A. K., Dover, L. G., Kremer, L., Besra, G. S., and Sacchettini, J. C. (2007) X-ray crystal structure of *Mycobacterium tuberculosis* β-ketoacyl acyl carrier protein synthase II (mtKasB). *J. Mol. Biol.* **366,** 469–480
14. Pan, H., Tsai, S., Meadows, E. S., Miercke, L. J., Keatinge-Clay, A. T., O'Connell, J., Khosla, C., and Stroud, R. M. (2002) Crystal structure of the priming β-ketosynthase from the R1128 polyketide biosynthetic pathway. *Structure* **10,** 1559–1568
15. Theisen, M. J., Misra, I., Saadat, D., Campobasso, N., Miziorko, H. M., and Harrison, D. H. (2004) 3-hydroxy-3-methylglutaryl-CoA synthase intermediate complex observed in "real-time." *Proc. Natl. Acad. Sci. U.S.A.* **101,** 16442–16447
16. Haapalainen, A. M., Meriläinen, G., and Wierenga, R. K. (2006) The thiolase superfamily: condensing enzymes with diverse reaction specificities. *Trends Biochem. Sci.* **31,** 64–71
17. Kresovic, D., Schempp, F., Cheikh-Ali, Z., and Bode, H. B. (2015) A novel and widespread class of ketosynthase is responsible for the head-to-head condensation of two acyl moieties in bacterial pyrone biosynthesis. *Beilstein J. Org. Chem.* **11,** 1412–1417
18. Alexson, S. E., and Nedergaard, J. (1988) A novel type of short- and medium-chain acyl-CoA hydrolases in brown adipose tissue mitochondria. *J. Biol. Chem.* **263,** 13564–13571
19. Ellman, G. L. (1958) A colorimetric method for determining low concentrations of mercaptans. *Arch. Biochem. Biophys.* **74,** 443–450
20. Musayev, F., Sachdeva, S., Scarsdale, J. N., Reynolds, K. A., and Wright, H. T. (2005) Crystal structure of a substrate complex of *Mycobacterium tuberculosis* β-ketoacyl-acyl carrier protein synthase III (FabH) with lauroyl-coenzyme A. *J. Mol. Biol.* **346,** 1313–1321
21. Price, A. C., Choi, K. H., Heath, R. J., Li, Z., White, S. W., and Rock, C. O. (2001) Inhibition of β-ketoacyl-acyl carrier protein synthases by thiolactomycin and cerulenin: structure and mechanism. *J. Biol. Chem.* **276,** 6551–6559
22. Olsen, J. G., Kadziola, A., von Wettstein-Knowles, P., Siggaard-Andersen, M., and Larsen, S. (2001) Structures of β-ketoacyl-acyl carrier protein synthase I complexed with fatty acids elucidate its catalytic machinery. *Structure* **9,** 233–243
23. Zhang, Y. M., Rao, M. S., Heath, R. J., Price, A. C., Olson, A. J., Rock, C. O., and White, S. W. (2001) Identification and analysis of the acyl carrier protein (ACP) docking site on β-ketoacyl-ACP synthase III. *J. Biol. Chem.* **276,** 8231–8238
24. Erol, O., Schäberle, T. F., Schmitz, A., Rachid, S., Gurgui, C., El Omari, M., Lohr, F., Kehraus, S., Piel, J., Müller, R., and König, G. M. (2010) Biosynthesis of the myxobacterial antibiotic corallopyronin A. *Chembiochem* **11,** 1253–1265
25. Sucipto, H., Wenzel, S. C., and Müller, R. (2013) Exploring chemical diversity of pyrone antibiotics: molecular basis of myxopyronin biosynthesis. *Chembiochem* **14,** 1581–1589
26. Sucipto, H., Sahner, J. H., Prusov, E., Wenzel, S. C., Hartmann, R. W., Koehnke, J., and Muller, R. (2015) *In vitro* reconstitution of alpha-pyrone ring formation in myxopyronin biosynthesis. *Chem. Sci.* **6,** 5076–5085
27. Miziorko, H. M., Shortle, D., and Lane, M. D. (1976) Trapping of a novel coenzyme A containing intermediate of 3-hydroxy-3-methylglutaryl-CoA synthase. *Biochem. Biophys. Res. Commun.* **69,** 92–98
28. Chester, N., and Marshak, D. R. (1993) Dimethyl sulfoxide-mediated primer Tm reduction: a method for analyzing the role of renaturation temperature in the polymerase chain reaction. *Anal. Biochem.* **209,** 284–290
29. Adams, P. D., Afonine, P. V., Bunkóczi, G., Chen, V. B., Davis, I. W., Echols, N., Headd, J. J., Hung, L. W., Kapral, G. J., Grosse-Kunstleve, R. W., McCoy, A. J., Moriarty, N. W., Oeffner, R., Read, R. J., Richardson, D. C., *et al.* (2010) PHENIX: a comprehensive Python-based system for macromolecular structure solution. *Acta Crystallogr. D Biol. Crystallogr.* **66,** 213–221
30. Emsley, P., Lohkamp, B., Scott, W. G., and Cowtan, K. (2010) Features and development of Coot. *Acta Crystallogr. D Biol. Crystallogr.* **66,** 486–501
31. Chen, V. B., Arendall, W. B., 3rd, Headd, J. J., Keedy, D. A., Immormino, R. M., Kapral, G. J., Murray, L. W., Richardson, J. S., and Richardson, D. C. (2010) MolProbity: all-atom structure validation for macromolecular crystallography. *Acta Crystallogr. D Biol. Crystallogr.* **66,** 12–21
32. Schrodinger, LLC (2015) The PyMOL Molecular Graphics System, version 1.8.05